Synthesis, characterization and third-order nonlinear optical properties of a dodecaruthenium organometallic dendrimer with a zinc(ii) tetraphenylporphyrin core

Areej Merhi, Guillaume Grelaud, Mahbod Morshedi, Seifallah Abid, Katy A Green, Adam Barlow, Thomas Groizard, Samia Kahlal, Jean-François Halet, Hoang Minh Ngo, et al.

Synthesis, Characterization and Third-Order Nonlinear Optical Properties of a Dodecaruthenium Organometallic Dendrimer with a Zinc(II) Tetra-phenylporphyrin Core

Areej Merhi,[a] Guillaume Grelaud,[a,b] Mahbod Morshedi,[b] Seyfallah Abid,[a] Katy A. Green,[b] Adam Barlow,[b] Thomas Groizard,[a] Samia Kahlal,[a] Jean-François Halet,*[a] Hoang Minh Ngo,[c] Isabelle Ledoux,[c] Marie P. Cifuentes,[b] Mark G. Humphrey,*[b] Frédéric Paul*[a] and Christine O. Paul-Roth*[a]

[a] Univ Rennes, INSA Rennes, CNRS, ISCR (Institut des Sciences Chimiques de Rennes) - UMR 6226, F-35000 Rennes, France.
[b] Research School of Chemistry, Australian National University, Canberra ACT 2601, Australia.
[c] LPQM, UMR CNRS 8537, ENS-Cachan, 61 avenue du président Wilson, 94230 Cachan, France.

A new Zn(II) porphyrin-based dendrimer (**5₂**) containing twelve Ru(II) alkynyl fragments, has been prepared following a convergent approach in two steps from 5,10,15,20-tetra(4-ethynylphenyl)porphyrinatozinc(II) (**6**). The cubic nonlinear optical (NLO) properties of **5₂** and other derivatives of **6** have been measured by third-harmonic generation (THG) at 1907 nm and by Z-scan over the spectral range 500-1700 nm, revealing the remarkable NLO response of **5₂** in the near-IR range. These results highlight the beneficial role of the extended "cross fourchée"-like polymetallic structure of **5₂** on its third-order NLO properties.

Introduction

Since the late 1980s, there has been an increasing interest in third-order nonlinear optical (NLO)-active molecules because of their promising potential for various technological applications.[1-2] Most of the initial work in this field was focused on developing molecular materials for all-optical information processing using NLO effects occurring on ultra-fast timescales.[3] As a result, molecules with high nonlinear refractive coefficients and minimal nonlinear absorption were initially developed, *i.e.* molecules for which the real part of γ (γ_{re}) is large at a given wavelength.[4] Subsequently, effects that occur on comparatively longer timescales such as saturable absorption (SA) or reverse saturable absorption (RSA) were also used for building optical gates or optical limiters.[5] More recently, cubic NLO effects that depend on the nonlinear absorption properties of molecules (related to the imaginary part of γ or γ_{im}) have also found application for other very important societal uses,[6] such as two-photon absorption (2PA) in optical data storage,[7] microfabrication,[8-9] fluorescence imaging or two-photon photodynamic therapy.[10-12] For all of these various NLO developments, organometallic derivatives have been identified as promising species, since they usually possess larger cubic polarizabilities than purely organic structures of similar size.[3, 13-20] In addition, when redox-active metal centres are present, organometallics offer the possibility of controlling the cubic NLO activity at specific wavelengths by electrochemistry.[21] However, in spite of these attractive perspectives, only a limited number of studies have thus far been performed on organometallic molecules in comparison to those conducted on organic structures, and most of these investigations were conducted at a single wavelength. Thus,

NLO studies on new organometallic structures at several wavelengths are now clearly desirable in order to further progress towards the elaboration of efficient organometallic molecular materials for cubic NLO applications.[22]
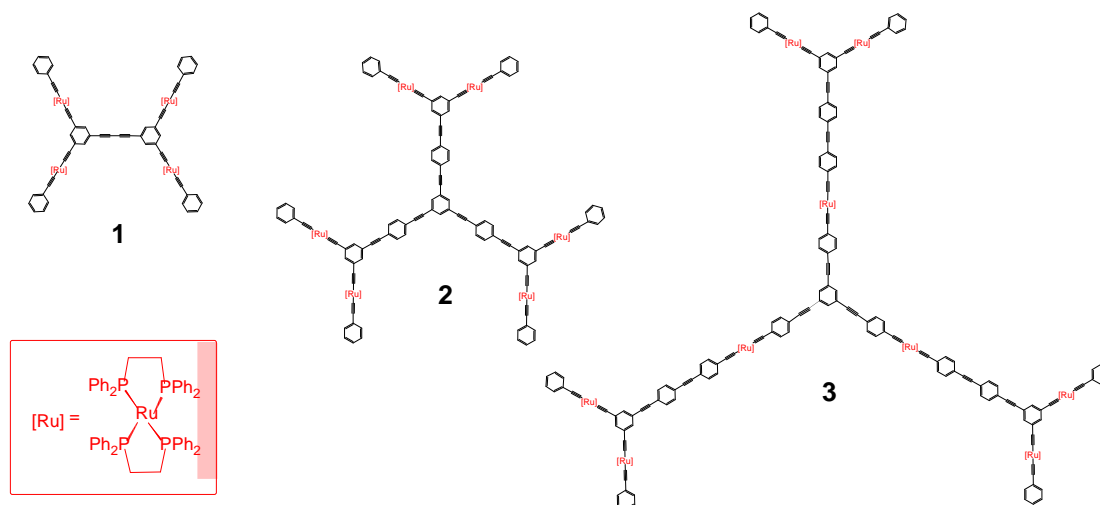

Chart 1. Some Ru(II)-containing organometallic dendrimers developed for cubic optical nonlinearity.

In this respect, organometallic dendrimers constructed from dendrons containing metal units such as *trans*-Ru(κ^2-dppe)$_2$ (dppe = 1,2-bis(diphenylphosphino)ethane) with bis-alkynyl ligation, and incorporated in an extended π-manifold, emerged recently as a particularly promising class of molecules (Chart 1).[20,23-24,‡] Indeed, nonlinear optical effects generally necessitate large and polarizable π-electron systems. Due to the inherent cooperativity between the various Ru(II) centres in a limited volume of space, comparatively high third-order optical nonlinearities were observed with this kind of three-dimensional structure. For instance, a dramatic increase in the 2PA cross-sections in the near-IR range was observed when proceeding from **1** to **2** and then to **3** (Scheme 1),[23] a 2PA cross-section of 11800 GM being reported at 750 nm for the last-mentioned dendrimer.[27]
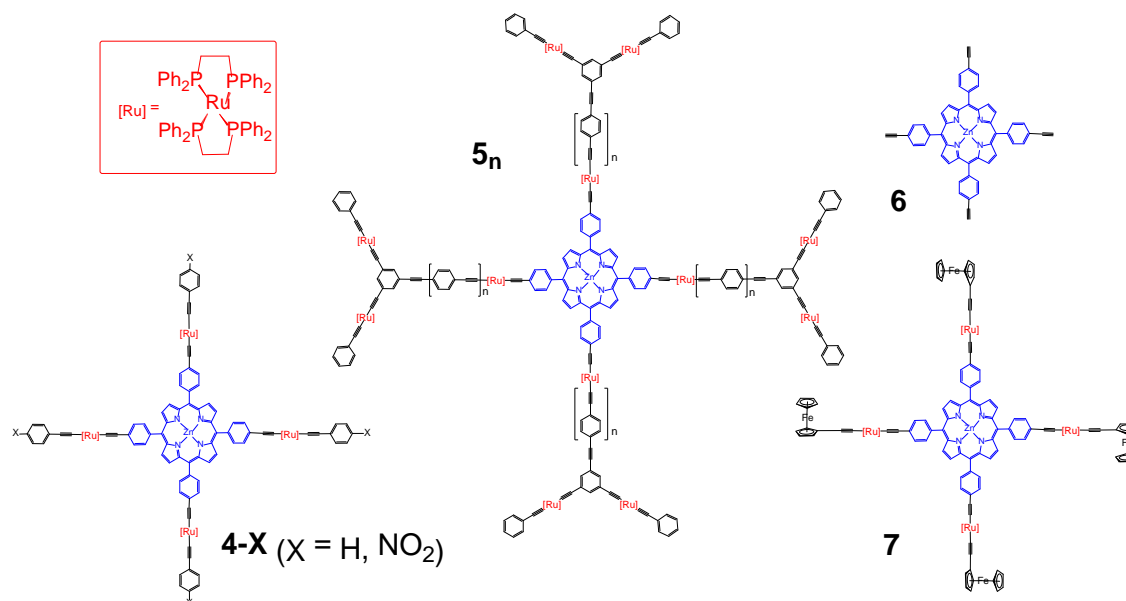

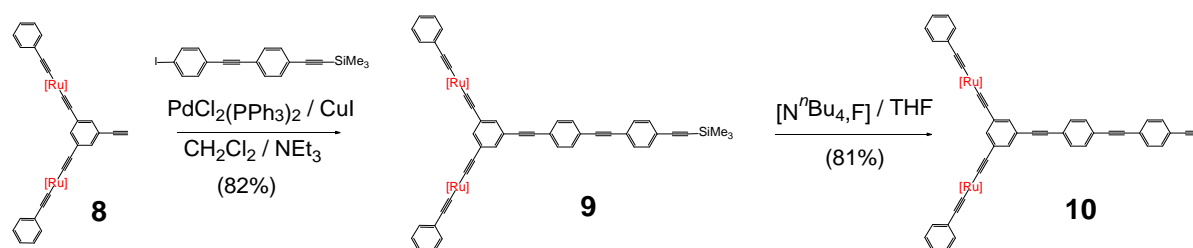**Chart 2.** Target molecule **5$_2$** and related compounds.

Independently from these investigations, large metallated π-architectures such as porphyrins and phthalocyanines were also identified as efficient and robust cubic NLO-phores.[28-33] Molecular materials based on these structures were therefore developed and used in various devices, such as optical gates[34] or optical limiters,[32, 35-36] for example. An attractive feature is that peripheral (*meso*) electron-releasing substituents on the macrocyclic core were shown to enhance the cubic NLO performance at 532 nm.[37] Thus, using zinc(II) tetraphenylporphyrin (ZnTPP) as a central (prototypical) core, we have recently shown that tetra-Ru(II) derivatives, such as **4-X** (Chart 2),[38-39] possess remarkable nonlinear absorptions around 550 nm and also in the near-IR range, relative to related unsubstituted porphyrins. In a continuation of these investigations, and inspired by the synthesis of related metal alkynyl-containing dendrimers[40] or porphyrins,[41] we have now undertaken the synthesis of the new compounds **5_n** (*n* = 1, 2) which contain four Ru(κ^2-dppe)$_2$-based dendrons at the *meso* positions.

We report herein the synthesis of **5_2** in a few steps from the known Zn(II) precursor **6**, its characterization, and an extensive investigation of its third-order NLO properties and those of the related complex **7**.[42] Some of these investigations have been previously communicated.[43] In particular, THG measurements indicated better NLO responses for **5_2** and **7** at 1907 nm, once the γ_{THG} values had been corrected for the molecular mass of the molecules. Presently, additional Z-scan measurements conducted between 500 and 1800 nm for these molecules give the spectral dependence of their NLO response on a broader frequency range and provide more insight on the impact of the structural changes between **4-X**, **5_n** and **7**.

Results and discussion

1. Synthesis of the porphyrin-based dendrimer 5$_2$.

Preparation of the diruthenium dendron **10** was carried out in an analogous fashion to the previously reported synthesis of the smaller homologue **8** (Scheme 1),[24, 44] itself obtained by reacting 1,3,5-triethynylbenzene with excess *cis*-[RuCl$_2$(κ^2-dppe)$_2$],[45] followed by a chloride for phenylalkynyl ligand metathesis.[44] Complex **10** was isolated in 66% overall yield from **8**.[§]

Scheme 1. Synthesis of the wedge **10**.

Synthesis of the porphyrin-based dendrimer **5_2** was subsequently undertaken by reacting four equivalents of **10** with the porphyrin precursor **11-v**[PF$_6$]$_4$.[50] Thus, rather than employing the tetra-chloroalkynyl Ru(II) complex **11** directly,[38-39] its *tetra*-vinylidene precursor **11-v**[PF$_6$]$_4$ was used. The latter was generated from the known tetraethynyl Zn(II) porphyrin **6** in the presence of a fourfold excess of *cis*-[RuCl$_2$(κ^2-dppe)$_2$] (4.1 eq.), precipitated from the reaction medium, and then directly engaged with a fourfold excess of the dinuclear wedge **10** (Scheme 2). The reaction was monitored by ^{31}P NMR spectroscopy, since it was accompanied by characteristic changes in the chemical shifts:

signals at 54.3 ppm and at 54.6 ppm corresponding to the desired product **5$_2$** appeared while the singlet corresponding to the (deprotonated) starting material **11**, at 51.0 ppm, decreased in intensity and eventually disappeared, indicating complete consumption of the starting porphyrin after 48 h.[§§] Compound **5$_2$** was then precipitated from hexane and isolated in 48% overall yield as a green solid after recrystalization in presence of 1 eq. Zn(OAc)$_2$•2H$_2$O to re-metallate any fraction of the product featuring a demetallated porphyrin ring. The new organometallic dendrimer **5$_2$** was fully characterized by means of IR, UV, and NMR spectroscopies, microanalysis, and cyclic voltammetry (CV), as described below. Characterization of this compound by mass spectrometry proved problematic, because the molar mass (13742.9 amu) exceeded the limits of the local ESI mass spectrometer. Only a cationic ion corresponding to a protonated fragment of one of the four branches of the compound (*i.e.* [*trans*-Ru(C≡CPh)(κ^2-dppe)$_2${C≡C(1,4-C$_6$H$_4$)C≡C-(1,4-C$_6$H$_4$)C≡C(1,4-C$_6$H$_4$)C≡C}-1,3,5-C$_6$H$_3${C≡C-*trans*-Ru(C≡C-Ph)(κ^2-dppe)$_2$}$_2$]$^+$ could be clearly characterized by HRMS. Nevertheless, this suggests that the desired coupling has taken place.

In contrast, and in line with previous observations,[27, 51] when this reaction was attempted with the shorter dendron **12**, no reaction at all took place. Thus, only the signatures of the free ligand (**12**) and of the deprotonated vinylidene (**11**) were detected (a singlet at 54.5 ppm and another at 51.0 ppm) after 24, 48, and 72 hours. Replacement of the dichloromethane solvent by THF and/or refluxing of the medium was not more rewarding. Once again, no reaction apparently took place between **11-v**[PF$_6$]$_4$/**11** and **12**. This result is tentatively attributed to the comparably larger steric hindrance at the site of reactivity in **12** relative to that in **10**.[#]

Scheme 2. Synthesis of **5$_2$**.

2. Characterization of the new porphyrin-based dendrimer 5$_2$

2.1. Spectroscopic characterization of 5$_2$. The two signals at *ca.* 54.3 and 54.6 ppm in the ^{31}P{^{1}H} NMR spectrum of **5$_2$** are diagnostic of the phosphorus atoms of *trans*-bis(alkynyl) "Ru(κ^2-dppe)$_2$" units.[27, 53] Based on their intensity, they correspond respectively to the chemically distinct inner (4) and peripheral (8) Ru(κ^2-dppe)$_2$ units present in **5$_2$**.[52] A similar chemical shift difference has been reported for the N-cored dendrimer **3** (Scheme 1) which is constructed from similar dendritic wedges.[18] Interestingly, high field NMR resolves these two signals and suggests that the phosphorus atoms belonging to the inner Ru(κ^2-dppe)$_2$ units actually correspond to an AB system. We tentatively attribute this to a slight chemical non-equivalency imparted to these phosphorus atoms by the semi-twisted ("gauche") conformation adopted by the peripheral *meso*-phenyl rings due to the presence of the bulky wedges. The ^{1}H NMR spectrum of this compound exhibits the characteristic signals of the central ZnTPP core and of the "Ru(κ^2-dppe)$_2$" units in the expected proportions, as indicated by the integration of the signal of the eight β-pyrrolic protons at *ca.* 9 ppm against that of the 96 methylene protons of the dppe groups at *ca.* 3 ppm. Moreover, the ^{1}H NMR spectrum also reveals the absence of the acetylenic proton previously observed for **10** at *ca.* 3.2 ppm, suggesting, in line with the HRMS spectrum, that the expected coupling has indeed taken place. The ^{1}C{^{1}H} NMR characterization of this compound was complicated by its poor solubility. Nevertheless, the spectrum clearly reveals the presence of "Ru(κ^2-dppe)$_2$" units, along with diagnostic resonances that might be assigned to the porphyrin and arylalkynyl units. Finally, IR confirms the presence of Ru(II) alkynyl linkages, which are revealed by the presence of a single and broad absorption at *ca.* 2050 cm^{-1} corresponding to the various overlapped $\nu_{RuC \equiv C}$ modes.[38] As seen previously with related bis-alkynyl Ru(II) compounds,[38] only one broad $\nu_{C \equiv C}$ band is usually observed in spite of the presence of two dissimilar alkynyl ligands at the Ru(II) centre. Thus, only one band was previously observed for **4-H** (at 2056 cm^{-1}) and for **7** (at *ca.* 2050 cm^{-1}). The second and less intense absorption observed for **5$_2$** at 2200 cm^{-1} most likely corresponds to the overlapped $\nu_{C \equiv C}$ modes of the tolane spacer (Table 1).[54]

2.2. Cyclic voltammetry studies. Cyclic voltammetry (CV) studies of the dendritic wedge complexes **9** and **10** were recorded in dichloromethane, with [NBu$_4$][PF$_6$] (0.1 M) as supporting electrolyte (Table 1). In line with published data for closely related wedges,[53] these compounds exhibit two overlapping chemically reversible oxidations ($\Delta E^0 \approx 0.11$ V) at *ca.* 0.42-0.53 V vs. SCE (see ESI), which can be difficult to resolve under standard conditions for some dendrimers.[20] Based on the CV data previously gathered for the shorter compound **4-H**,[38] one Ru-centred oxidation and several porphyrin-centred oxidations were additionally expected at *ca.* 0.45 V and at potentials above 0.9 V, respectively. Accordingly, the voltammogram of **5$_2$** recorded under similar conditions possesses these features but the porphyrin-based waves, close to the solvent edges, were difficult to detect.[43] To improve their detection, the CV was then recorded in THF which offered a slightly larger potential window. Six oxidation waves were detected (Figure 1) for which differential pulse voltammetry (DPV) gives the approximate ratio 1:1:8:4:1:($\geq$)8. Thus, contrary to our earlier proposal,[43] the Ru(II)/Ru(III) oxidations of the peripheral and inner *trans*-Ru(κ^2-dppe)$_2$ fragments possibly overlap. Based on their intensity in a two-to-one ratio, the first oxidation of the Ru(II) centres belonging to the carbon-rich wedges[24] are apparently not resolved from that of the chemically distinct Ru(II) centres closer to the porphyrin core in **5$_2$**. Considering the previous results obtained for **4-X**,[56] **7**[42] and related compounds,[39, 57] oxidations taking place at more negative and more positive potentials are also

expected for the first and second reduction/oxidations of the metallated porphyrin core. Much weaker waves potentially corresponding to these 1-electron processes can be detected at -1.57, -1.21 and 1.08 V *vs.* SCE. Thus, two reductions and one oxidation of the ZnTPP core are also possibly observed, but these values should be taken with caution given that scanning to these potentials leads to chemical irreversibility with some deposition at the electrode. Finally, the many-electron oxidation detected around 1.38 V can be attributed to a second Ru-localized oxidation, based on its similarity with a process observed for the compound **7** at related potential values.[42] Here also, its chemical irreversibility complicates a more thorough analysis of this process. In contrast, the first Ru(II/III) oxidations take place in a reversible way (see ESI). Based on the CV, the quite similar oxidation potentials found for four of the eight peripheral bis-alkynyl Ru(κ^2-dppe)$_2$ units (0.42 V) and for the four inner Ru(κ^2-dppe)$_2$ units (0.46 V), suggests a very similar electronic environment around these units in **5$_2$**, in line with their overlapping phosphorus NMR resonances. Similar to previous observations with **7** and **4-H**,[42, 56] the chemical reversibility of these first Ru(II)-centred oxidations and their potential difference (*ca.* 70 mV) opens the possibility of using them for switching the NLO properties of **5$_2$**.[21, 58-60]

Table 1. Characteristic IR, ^{31}P NMR and cyclic voltammetric data for compounds **4-H**, **5$_2$** and **7**, and organometallic dendrons **9** and **10**.

Cmpd	IR[a] (cm^{-1})	^{31}P{^{1}H} NMR (ppm)[b]	E° (V vs. SCE)[c]	
			E° M(II/III)	E°$_1$ - E°$_3$ [ZnTPP]
4-H	2056	55.2	0.46	0.88, 1.21
5$_2$	2200 2051	54.6, 54.3	0.45, 0.53 [d]0.55, 0.62	/ / 0.95 -1.57, -1.21, 1.08
7[e]	2052	54.5	0.18, 0.76	/
9	2202 2155 2054	54.5	0.42, 0.52 [d]0.60, 0.68	/
10[f]	2198 2049	53.9	0.42, 0.53	/

[a] In KBr pellets; $\nu_{C\equiv C}$ modes only. [b] CDCl$_3$ or C$_6$D$_6$ (**7**). [c] CH$_2$Cl$_2$, 20 °C, 0.1 M [NBu$_4$][PF$_6$], scan rate 0.1 V.s-1 with ferrocene used as an external calibrant (M = Ru, Fc).[55] Potentials are expressed relative to that of the saturated calomel electrode (SCE). [d] Idem in THF. [e] From ref.[42] [f] See also Supporting Information of ref. [18].
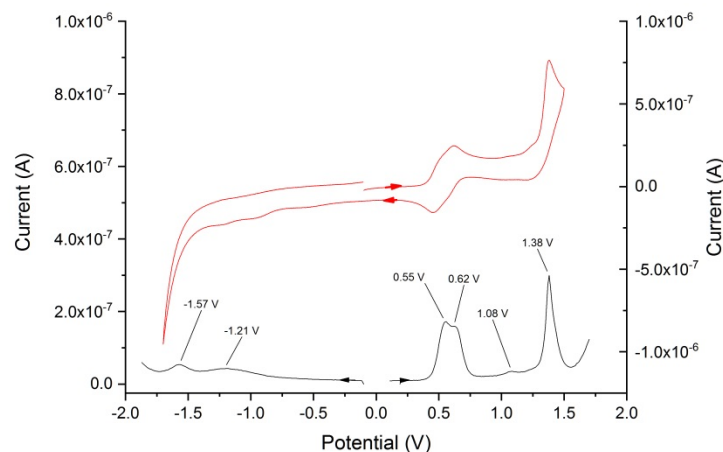
Figure 1. Cyclic voltammogram (in red) of the zinc porphyrin 5_2 in THF/[NBu$_4$][PF$_6$] (0.1 M) at 25 °C at 0.1 V/s between -1.6 and 1.4 V vs. SCE. The differential pulse voltammetry (DPV) trace (in black) is drawn below the cyclic voltammogram.

2.3. UV-Visible Spectroscopy. The UV-vis absorption spectrum of 5_2 was recorded and compared to that of compound **4-H** (Figure 2). It contains a Soret band at 420 nm with a shoulder at 460 nm and two Q bands at 562 and 612 nm. In addition, we observed an absorption band centred around 338 nm, which can be attributed to a $\pi^* \leftarrow d$ MLCT from the metal orbitals to the orbitals of the phenylalkynyl ligand, and diagnostic of the presence of *trans*-Ru(κ^2-dppe)$_2$ units in 5_2. This band was previously observed at 330 nm (142 000 mol^{-1}.dm^3.cm^{-1}) for **4-H** and at 340 nm (137 000 mol^{-1}.dm^3.cm^{-1}) for the dendron **9**. Relative to the Soret band, this band is now more intense than it was in **4-H**, consistent with the increased number of Ru(κ^2-dppe)$_2$ fragments present in 5_2 (four dendritic wedges). Despite its structure-less envelope, this band results from the overlap of MLCT transitions taking place at the "inner" and "outer" Ru(II) centres (see Theoretical studies section). The slight red shift of 8 nm undergone by this band when progressing from **4-H** to 5_2 might be rationalized as arising from the extension of the π-manifold.[23]
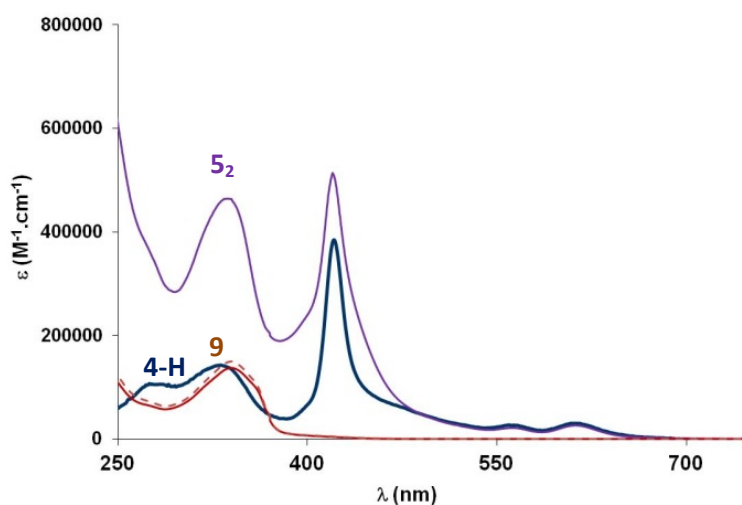

Figure 2. UV-vis absorption spectra of the zinc(II) porphyrin **4-H** and 5_2 and of the organometallic wedge **9** in CH$_2$Cl$_2$ at 25 °C.

Table 2. Experimental UV-vis absorption maxima in CH_2Cl_2.

Cmpd	λ_{max} (nm) / $[\varepsilon_{max}]$ (10^4 $M^{-1}.cm^{-1}$)
4-H [a]	330 [14.2], 421 [38.5], 460 [sh, 7.4], 563 [2.7], 612 [3.0]
4-NO$_2$ [b]	322 [7.7], 420 [24.8], 466 [sh, 10.4], 556 [4.2], 607 [3.0]
5$_2$	338 [46.4], 420 [51.4], 460 [11.4], 562 [2.1], 612 [2.6]
6 [a]	303 [2.4], 424 [55.6], 552 [2.3], 594 [0.6]
7 [c]	334 [9.3], 420 [36.8], 470 [sh, 5.6], 562 [2.6], 612 [3.2]
9	341 [13.7], 360 [sh, 9.6]
10	340 [14.3], 360 [sh, 10.4]

[a] UV-vis data remeasured. [b] Ref. [56] [c] Ref. [42]

3. Theoretical studies

Density functional theory (DFT) calculations were performed to provide some insight into the compound structures and the UV-vis absorption spectra. Compound **6** and models of compounds **4-H**, **5$_2$** and **9** (**4-H'**, **5$_2$'** and **9'**, respectively, in which Ru(dppe)$_2$ fragments were replaced by Ru(dpe)$_2$ (dpe = di(phosphino)ethane) to reduce computational effort) were considered. Note that the dppe replacement by dpe in large systems is common and often leads to minor changes in compound geometry and electronic properties.[61] Geometries were first optimized (Figure 3). Selected bond lengths are given in Table 3 (see Figure 4 for atom labeling). Distances computed for the porphyrin core in the different molecules compare very well with those measured experimentally in closely related molecules.[39, 62] Ru-P, Ru-C and C≡C distances in the Ru(II) alkynyl fragments are in the usual range found for related carbon chain-containing organometallic compounds in the literature.[63-64] This gives confidence in the computed bond distances in our compounds for which no X-ray data are available. Addition of external Ru(dpe)$_2$(C≡CPh)- entities in **4-H'** with respect to **6** hardly impacts the geometrical features of the porphyrin core.

The molecular orbital (MO) diagram of the tetraethynyl Zn(II) porphyrin **6** (Figure S10, ESI) indicates that the HOMO, HOMO-1, LUMO and LUMO+1 frontier orbitals are of the π type and mostly localized over the porphyrin ring, with hardly any participation of the central Zn. A weak participation of the phenyl-ethynyl branches is seen in the HOMO. A substantial HOMO-LUMO gap of 2.73 eV is computed at the B3PW91 level of theory. The LUMO and LUMO+1 of the dendrimers **4-H'** and **5$_2$'** (Figures S11 and S12, ESI) are similar in shape to those of the parent porphyrin **6** with negligible variation of atomic participation. A slight energy destabilization, *ca.* 0.2 eV, is noted. HOMOs in **4-H'** and **5$_2$'** show identical nodal properties, being highly weighed on the phenyl-ethynyl Ru fragment tethered to the porphyrin core. They lie at high energy due to their Ru-C antibonding character, intercalating above the occupied MOs of the porphyrin core. This leads to a diminution of the HOMO-LUMO gap of *ca.* 0.30 eV with respect to compound **6**. In **4-H'**, a set of several MOs delocalized over the organometallic branches are found. In the dendrimer **5$_2$'**, the HOMO-1 is one component of a bundle made of four nearly-degenerate antibonding orbitals, each localised on the remote part of one branch. Finally, a comparable HOMO-LUMO gap (2.75 eV) is computed for **9'** with HOMOs localized on the Ru-containing branches and LUMOs localized on the organic branch

(Figure S13, ESI). A comparable MO picture is computed for the real compound **9** (Figure S14, ESI) with a HOMO-LUMO gap (2.51 eV) slightly smaller than that computed for its model **9'**. All this gives support to the first oxidation(s) of the compounds **4-H'** and **5₂'** taking place in MOs with a strong ruthenium character, in line with their formal attribution as metal-centred oxidation processes.
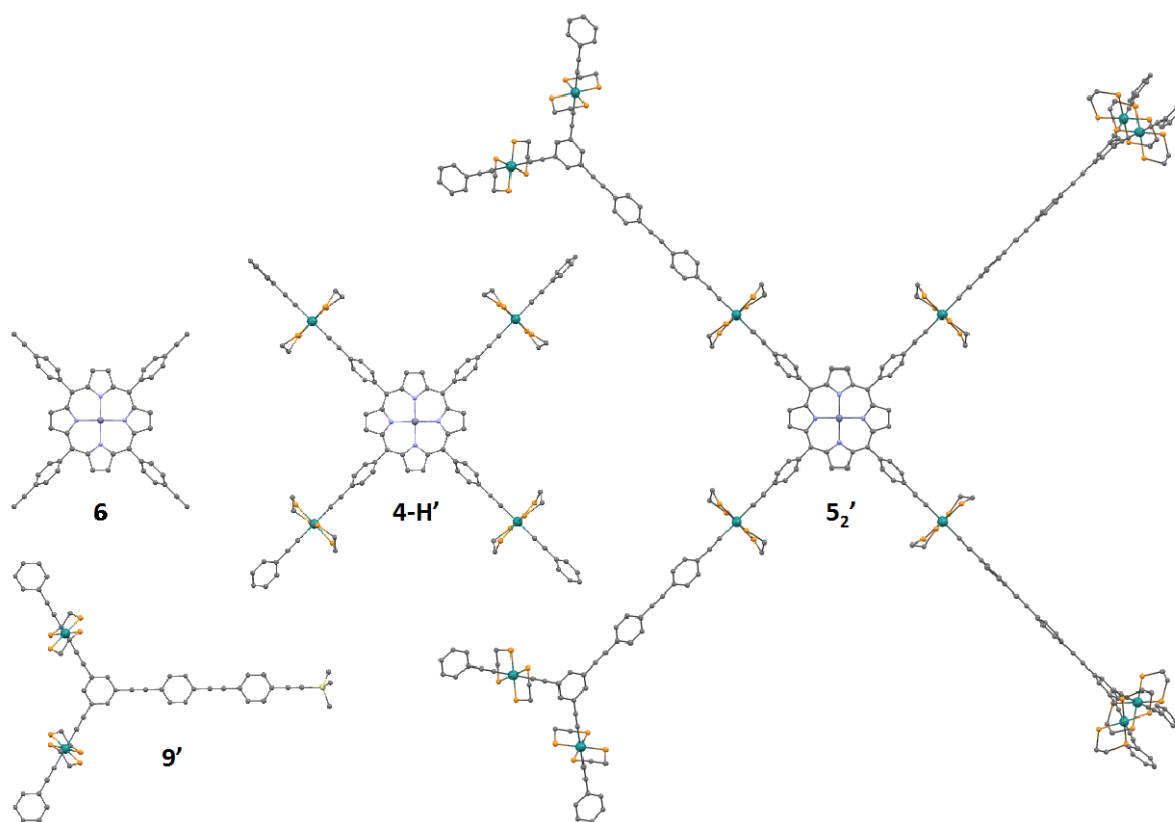

Figure 3. Optimized structures of **6** (top left), **4-H'** (middle), **5₂'** (right) and **9'** (bottom left). Hydrogen atoms are omitted for clarity.

Table 3. Selected bond lengths (Å) for compounds **4-H'**, **5₂'**, **6**, and **9'**. See Figure 4 for atom labelling.

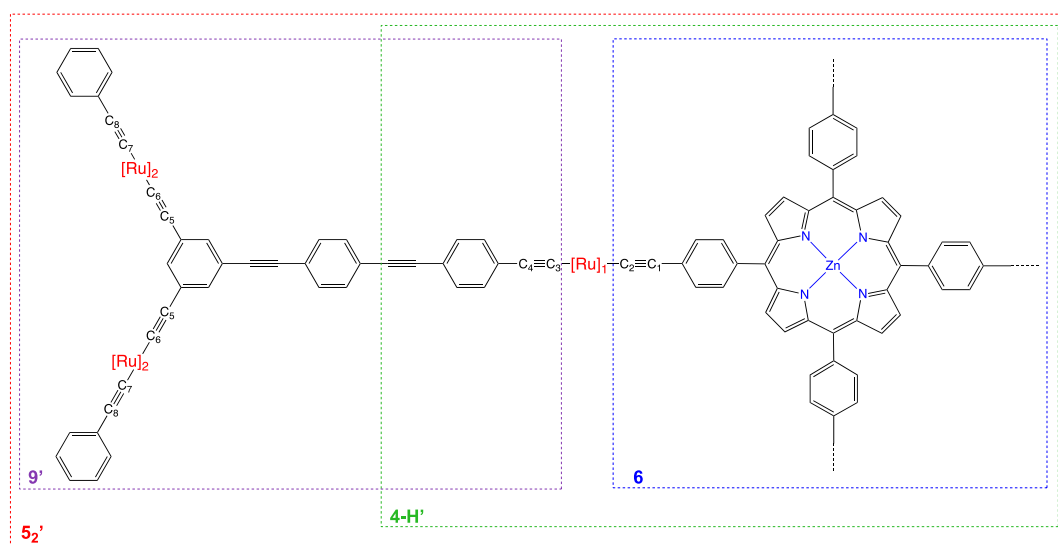| Compound	6	9'	4-H'	5₂'
Zn-N	2.057	–	2.057	2.057
$C_1 \equiv C_2$	1.215	–	1.237	1.237
C_2-Ru_1	–	–	2.052	2.053
Ru_1-P	–	–	2.311	2.312
Ru_1-C_3	–	–	2.053	2.049
$C_3 \equiv C_4$	–	1.226	1.236	1.237
$C_5 \equiv C_6$	–	1.236	–	1.236
C_6-Ru_2	–	2.054	–	2.054
Ru_2-P	–	2.311	–	2.311
Ru_2-C_7	–	2.053	–	2.053
$C_7 \equiv C_8$	–	1.236	–	1.236

Figure 4. Atom labeling in compounds **4-H'**, **5₂'**, **6** and **9'** ([Ru] = Ru(dpe)₂).
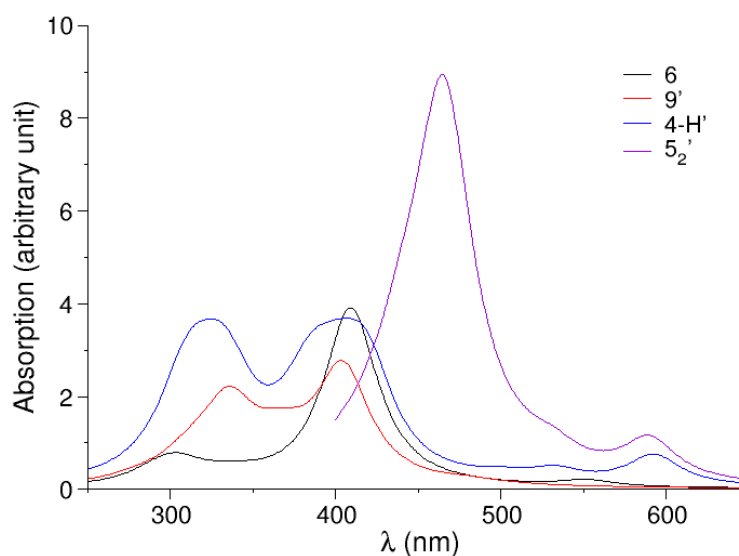

Figure 5. Calculated UV-vis absorption spectra of the compounds **4-H'**, **5₂'**, **6**, and **9'**. Computations were carried out up to 400 nm for **5₂'** due to computational limitations.

Time-dependent (TD)-DFT energies of the lowest allowed electronic excitations of **6**, **5₂'**, **4-H'** and **9'** were computed. They are shown in Figure 5 and compared in Table 4. A reasonable agreement between the simulated and experimentally measured spectra for **6** is observed with the Q-band and the Soret band computed at 552 and 409 nm, respectively. Corresponding experimental values were found at 552 and 424 nm, respectively (compare Tables 2 and 4). These electronic excitations involve HOMO/HOMO-1→LUMO/LUMO+1 ($\pi^* \leftarrow \pi$) electronic transitions usually observed for systems containing a porphyrin core.[65] The last electronic excitation computed at 303 nm is also due to a $\pi^* \leftarrow \pi$ transition but from the deep energy orbital HOMO-10 to LUMO/LUMO+1.
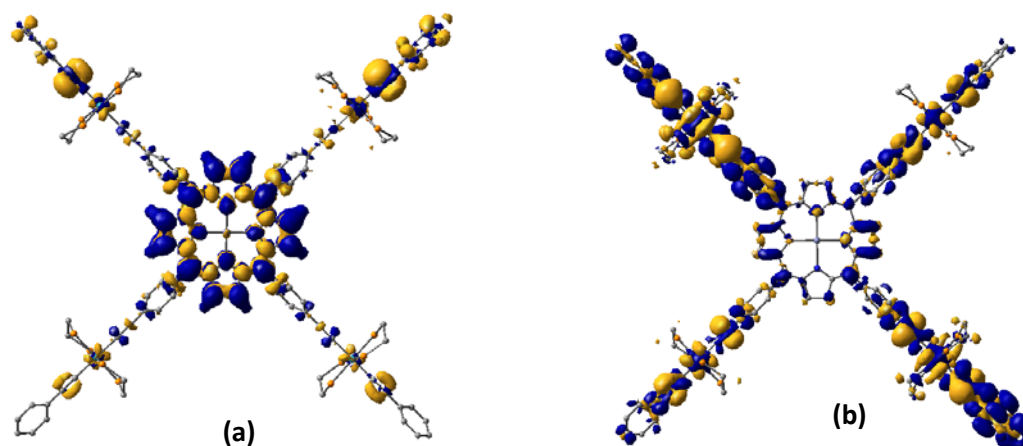
Figure 6. Density-difference plot associated with a) the Soret band and b) the MLCT band λ = 332 nm in **4-H'**. The blue and yellow colours indicate an increase and decrease of density upon excitation, respectively [isocontour value = 0.0002 e.bohr^{-3}].

Similar Q-band absorptions are computed for **4-H'** and **5$_2$'** with a noticeable red shift of about 40 nm compared to that computed for **6** (see Figure 5 and Table 4). This is expected since these bands involve electronic transitions between HOMO and LUMO that are less separated in energy than in **6** and show comparable energies and composition. In **4-H'** the Soret band computed at 419 nm (10 nm red shifted vs. that in **6**) corresponds to electronic transitions dominated mostly by charge transfer inside the porphyrin moiety with some admixture of the Ru-containing branches (see the density-difference plot in Figure 6a). A rather broad absorption peak is also computed around 330 nm (see Figure 5 and Table 4). This corresponds to an important metal-to-ligand charge transfer (MLCT) transition as shown by the density-difference plot of the band found at 332 nm (Figure 6b). Actually, it is a sum of several symmetry-allowed transitions where electronic density located on the four ruthenium centres is redistributed in π^* MOs located on the inner and peripheral alkynyl ligands, as well as on the central porphyrin ring. A very intense absorption band at 465 nm is computed for **5$_2$'**. This corresponds to the Soret band which is somewhat red shifted (*ca.* 45 nm) compared to that computed for **6** and **4-H'**. Multiple electronic transitions are involved implying charge transfer over the whole molecule. Overall, the agreement between the computed spectra of **4-H'** and **5$_2$'** and the experimental ones of **4-H** and **5$_2$** is satisfactory.

Table 4. Computed absorption λ_{max} (nm) and oscillator strength *(f)* for the compounds **4-H'**, **5$_2$'**, **6**, and **9'**.

Cmpd	λ_{max} [f]
4-H'	311 [0.63] 332 [0.43] 383 [0.66] 393 [0.48] 403 [0.43] 419 [1.06] 501 [0.06] 534 [0.10] 593 [0.34]
5$_2$'^{a}	406 [0.15] 429 [0.20] 442 [0.43] 465 [3.60] 479 [0.16] 507 [0.06] 531 [0.22] 590 [0.43]
6	303 [0.23] 409 [1.95] 552 [0.07]
9'	336 [1.45] 368 [0.57] 404 [2.46]

^{a} Computed up to 400 nm due to computational limitations.

Moderate agreement between the simulated spectrum of **9'** and the experimentally measured UV−vis spectrum of **9** is observed. The rather intense lowest energy absorption at 404 nm involves mostly some charge transfer from the Ru-alkynyl units to the organic branch. Indeed, the red shift of the computed absorptions in **9'** with respect to the absorption bands at 340-360 nm experimentally measured in **9** is mainly due to the planarity of the former which is less sterically hindered than the latter. An intense electronic excitation is computed at 336 nm which might correspond to that experimentally observed at 340 nm in **9**. A look at the main electronic transitions responsible for this absorption band (Figure S15, ESI) indicates important MLCT character but also some ligand-to-ligand charge transfer (LLCT) character.

4. Nonlinear optical properties of 5₂ and 7

4.1. THG Measurements. The molecular third-order nonlinearities (γ_{THG}) of **4-X** (X = NO$_2$, H), **5$_2$**, **6a-b**, **7** and **9** were determined from third-harmonic generation (THG) studies at 1907 nm (Table 5). As previously mentioned,[42] the THG data at 1907 nm are almost certainly influenced by resonance enhancement of the third-harmonic response at 635 nm due to proximity to the lowest energy Q band. The γ_{THG} value for **5$_2$** is much larger in magnitude than that of **6** or that of the smaller porphyrin derivatives **4-X** (X = H, NO$_2$) or **7**, emphasizing the importance of the extension of the π-manifold and incorporation of transition metal atoms in its peripheral branches. It is also much larger than four times the γ_{THG} value for the dendritic wedge **9** added to that of the metallated core **6**, suggesting considerable synergy between these fragments contributing to the observed THG response of **5$_2$**. When the γ_{THG} values obtained from the present studies are divided by the molecular weight of the chromophore, a comparable value is found for **5$_2$** relative to **4-H**, but this value is lower than that of **7**. This indicates that these resonance-enhanced γ_{THG} values determined at 1907 nm broadly correlate with the spatial extension of the conjugated π-manifold in **5$_2$** and **4-H**. However, even on the basis of such figures of merit, **7** seems more active, which suggests that the inclusion of d^6-transition metal centres in positions conjugated with the peripheral Ru(II) atoms, as in **7**, is more beneficial for THG merit than appending extended organometallic wedges containing more Ru(II) centres but in non-conjugated (and more remote) positions from these atoms, as in **5$_2$**. Investigation of the frequency dependence of the cubic NLO response will afford additional information regarding this statement. In this respect, the relative constancy observed for the Ru(II/III) oxidation potentials, for the $\bar{\upsilon}_{C\equiv CRu}$ stretching modes and for the energy of the $\pi^* \leftarrow d_{Ru}$ MLCT bands in these compounds points to a similar polarization of the -C≡C-Ru-C≡C- fragments, suggesting that the better NLO response of **7** cannot be related to significant bonding changes taking place in the peripheral branches of all these compounds in their ground state.
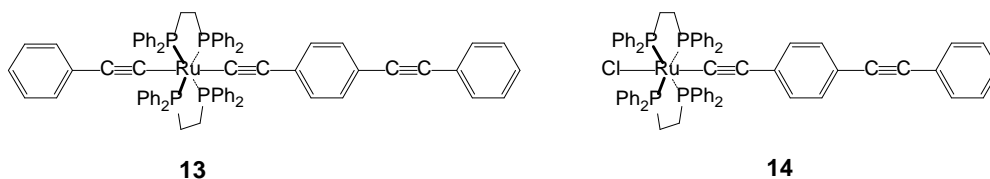

13   **14**

Chart 3. Related complexes previously assessed by femtosecond Z-scan.[17]

Table 5. $\gamma_{THG}{}^{a}$ values at 1907 nm in CHCl$_3$.

Cmpd	λ_{max} (nm) [ε_{max}] ^{b}	$\varepsilon_{635\,nm}$ ^{b} (M^{-1}.cm^{-1})	γ_{THG} ^{a} (10^{-34} esu)	γ_{THG}/M ^{c} (10^{-34} esu)
4-H	612 [3.0]	1.5	-550	-0.115
4-NO$_2$	607 [3.0]	0.9	-170	-0.034
5$_2$	612 [2.6]	1.1	-1840	-0.134
6	594 [0.6]	0.3	-13	-0.016
7	612 [3.2]	1.8	-1080	-0.208
9	360 [sh, 12.0]	0.0	+24	-0.010

^{a} Cubic hyperpolarizabilities (± 10%) obtained from a THG experiment.[43] ^{b} Lowest energy absorption and extinction coefficients in 10^4 M^{-1}.cm^{-1}. ^{c} Molecular cubic hyperpolarizabilities corrected for the molecular mass (M) in g.mol^{-1}.

4.2. Z-Scan Measurements for 5$_2$ and 7. We have determined nonlinear absorption, nonlinear refraction and |γ| values for **5$_2$** and **7** (Figure 7 and ESI) in the 500-1700 nm range by femtosecond Z-scan studies. Nonlinear refraction (γ_{re}) appears to dominate the cubic NLO response over the full spectral range probed, corresponding to an overall negative coefficient, in line with the previous THG measurement at 1907 nm. The γ_{re} values are therefore negative and consistently larger in magnitude than the nonlinear absorption coefficients (γ_{im}). When the cubic nonlinearity of **5$_2$** is compared to those previously determined for the mononuclear complexes **13** (|γ| = 15 x 10^{-34} esu) and **14** (|γ| = 4.6 x 10^{-34} esu) at 800 nm (Chart 3),[17] at a similar wavelength, an increase of roughly three orders of magnitude in the resulting γ value for **5$_2$** (4300 x 10^{-34} esu) is observed, possibly reflecting the positive influence of the extended π-manifold and polymetallic nature of this compound on the cubic nonlinearities. However, care must be paid here since the spectral dependence of the NLO response of these complexes was not established, and thus their values at 800 nm perhaps do not correspond to an extremum, as is the case for **5$_2$**. When compared to the data previously obtained for **7** at various wavelengths in the near-IR range (> 800 nm), similar spectral shapes are observed (ESI), but the |γ| values are in general two to three times larger for **5$_2$** (Table 6). Not surprisingly, **5$_2$** also performs much better than the dendrimer **3** (|γ| = 290 x 10^{-34} esu) at 850 nm,[27] as the latter contains only three analogous dendrons instead of four in **5$_2$**. The large differences between the |γ| values are also consistent with a strong positive influence of the metallated-porphyrin core on the cubic polarizabilities.

As was observed with the THG values, correcting the Z-scan-derived |γ| values around 600 nm for the molecular masses of the molecules (taken as a simplistic method to gauge the size of the π-manifold) reveals that there is a clear improvement in molecular mass-caled |γ| when proceeding from **4-H** to **7**, but the gain is less obvious (within experimental error) when proceeding from **7** to **5$_2$**. Thus, in contrast to the figures of merit obtained from the THG data, no clear advantage is seen for **7** over **5$_2$** from these |γ|/M values in the 800-1700 nm range, the previous effect deriving perhaps from a better resonance enhancement with the second Q band (at 612 nm) taking place for **7** at 1907 nm.
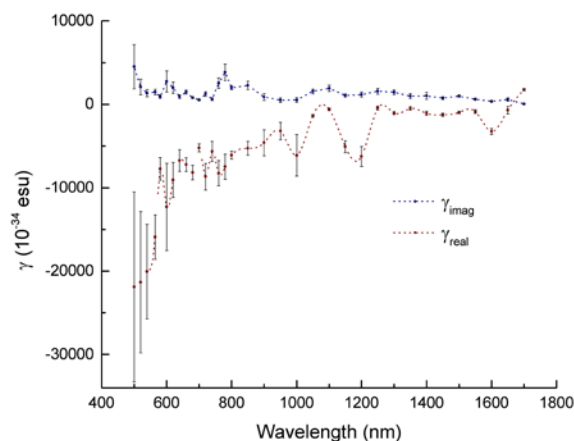
Figure 7. Plots of the real (red) and imaginary (blue) components of the second hyper-polarizability for **5₂.**

Table 6. Experimental γ_{re}, γ_{im}, $|\gamma|$ and σ_2 values at selected wavelengths[a] corresponding to extrema of the nonlinear absorption spectra of **5₂** and **7** compared to those previously obtained for **4-H**.[38]

Cmpd	λ[b]	γ_{re}[c]	γ_{im}[c]	$\mid\gamma\mid$[c]	$[\mid\gamma\mid/M]$[d]	σ_2[e]	$[\sigma_2/M]$[d]
4-H	620	-71 ± 7	-8.2 ± 1.0	71 ± 7	-0.015	-3400 ± 400	0.72
	710	/	/	/	/	4800 ± 500	1.00
	1130	/	/	/	/	1000 ± 500	0.21
	1300	/	/	/	/	1400 ± 500	0.29
5₂	600	-1230 ± 698	274 ± 168	1260 ± 718	0.091	118313 ± 55200	8.6
	780	-747 ± 151	383 ± 98	839 ± 180	0.061	97790 ± 24900	7.1
	1100	-61 ± 15	191 ± 38	200 ± 40	0.017	24500 ± 4800	1.78
	1250	-43 ± 23	156 ± 34	162 ± 41	0.012	15580 ± 3380	1.13
7	580	-465 ± 97	245 ± 62	525 ± 115	0.101	112700 ± 28600	21.6
	760	-205 ± 194	73 ± 17	217 ± 195	0.041	19480 ± 4650	3.7
	1100	-56 ± 11	15 ± 4	58 ± 12	0.011	1940 ± 570	0.37
	1250	-79 ± 9	21 ± 4	81 ± 10	0.016	2130 ± 420	0.41

[a] Conditions: measurements were carried out in CH_2Cl_2; γ values are referenced to the nonlinear refractive index of silica n_2 = 2.92 × 10-16 cm^2 W^{-1}. [b] Wavelength of the laser in nm. [c] 10^{-33} esu. The SI units for γ are $C.m^4.V^{-3}$, while those in the cgs system (used almost exclusively in the literature, and so given here) are $cm^5.statV^{-2}$ or esu. To convert between the two systems, $\gamma_{SI} = (1/3)^4 \times 10^{-23} \gamma_{cgs}$. [d] $|\gamma|$ and $|\sigma_2|$ corrected for the molecular mass (M) in $g.mol^{-1}$. [e] Effective (apparent) 2PA cross-section in Göppert-Mayer units (1 GM = 1 × 10^{-50} $cm^4.s.photon^{-1}$).

Given the importance of the nonlinear absorption properties of porphyrins or phthalocyanines for various applications,[32, 34, 36] the evolution of the apparent two-photon absorption (2PA) cross-section has been examined more closely for **4-H**,[38] **5₂** and **7** (ESI). The (effective/apparent) nonlinear absorption cross-sections (σ_2) have been extracted from γ_{im} values and were compared to the linear spectra plotted at twice their wavelength (Figure 8).[6] The spectra obtained for the three compounds are qualitatively very similar, but the 2PA cross-sections derived for **5₂** are always larger than those of **7**, themselves larger than those of **4-H**, as is apparent from the values given in Table 6. When plotted against the absorption

spectra at twice the wavelength, the maxima in the region where nonlinear absorption takes place (≥ 650 nm) roughly match the Soret and Q bands, suggesting that 2PA in these excited states takes place, and is more efficient for **5₂** than for **7**. A qualitatively similar situation can also be seen for **4-H** and **7** (Table 6) but lower in magnitude.[38] Finally, another maximum is located near 600 nm where linear absorption takes place in the lowest energy Q band. Such a situation calls for caution in interpretation of the data, since any 2PA might be convoluted with excited-state absorption phenomena, such as saturable absorption (SA) or reverse saturable absorption (RSA).[28] Positive values are found for **5₂** at 630 nm whereas negative values have been previously found for **4-H**, but these differences might be due to the slightly different acquisition conditions and laser pulses used.[38,±]

More importantly, 2PA is clearly enhanced above 800 nm for **5₂** compared to **4-H** and **7**, an improvement that might again be attributed to the extended π-manifold of the former compound. Note that no third-order NLO activity was detected for ZnTPP at 1024 nm using dark field Z-scan (DFZ-scan) by Boudebs *et al.*[28] Further, a huge increase is noted for **5₂** and **7** when compared to the 2PA cross-sections reported for the model alkynyl-metal complexes **13** (310 ± 50 GM) and **14** (110 ± 50 GM) at 800 nm,[17,60] a wavelength which nearly corresponds to 2PA in the MLCT state for all these compounds (*i.e.*, nearly twice the wavelength of the MLCT band). Also, **5₂** shows twice the 2PA merit of dendrimer **3** (Chart 1) at 750 nm (σ_2 = 11600 GM).[27]
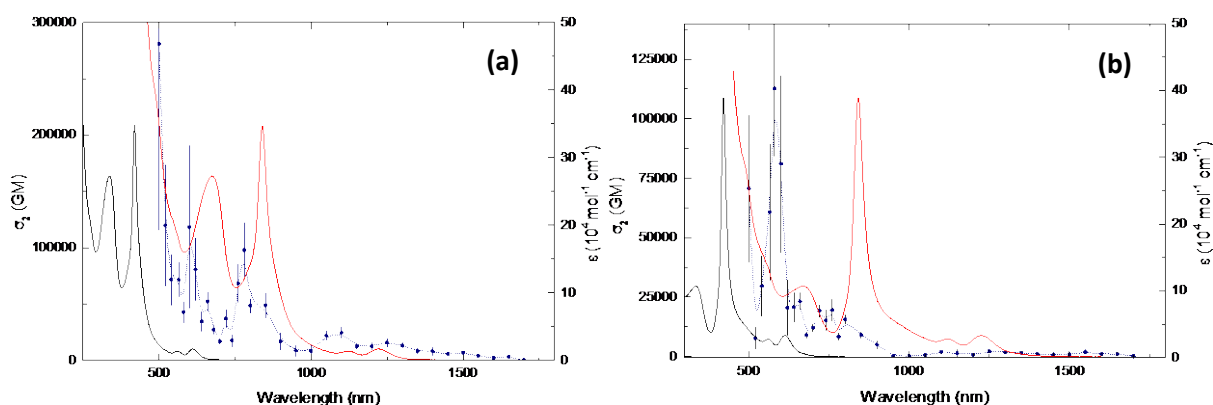

Figure 8. Two-photon absorption cross-section plots for **5₂** (a) and **7** (b) with trendline as a visual aid (blue) overlaid on one-photon absorption (OPA) spectra (black) and the same OPA plotted at twice the wavelength.

Correcting σ_2 values for the molecular mass of the molecules reveals that there is an improvement in these values for each local maximum when proceeding from **4-H** to **7** to **5₂**. In contrast to what was observed for $|\gamma|$ values, these figures of merit indicate that effective 2PA in the near-IR range is clearly more efficient for **5₂** than for the other two compounds. Thus, for potential applications for which nonlinear absorption has to be minimized and nonlinear refraction maximized,[66] such as for all-optical switching, smaller and more conjugated porphyrin-based architectures such as **7** will be more attractive, whereas for applications relying on maximum absorption, such as optical power limiting for instance,[67] extended structures such as **5₂** are clearly more interesting.

Conclusion

We have reported herein the synthesis and characterization of a new cross-shaped organometallic porphyrin-based dendrimer (**5₂**) containing twelve Ru(κ^2-dppe)₂ fragments. The dendrimer has been isolated in fair yield in one step, by reacting four preformed alkyne-terminated organo-ruthenium (II) dendrons with the hetero-pentametallic tetra-vinylidene complex **11-v**[PF₆]₄. The resulting metallo-dendrimer **5₂** was characterized by spectroscopic and voltammetric means. Compared to its shorter homologue **4-H** containing four Ru(κ^2-dppe)₂ fragments, the presence of the eight additional organoruthenium units at the periphery is clearly manifested by a new chemically reversible Ru(III/II) redox process in the cyclic voltammogram and by a fourfold increase in the intensity of the MLCT band near 330 nm in its absorption spectrum. A significant improvement in cubic NLO properties on proceeding from the dendritic wedges or porphyrin core to the dendrimer was observed by both THG and Z-scan. The refractive component of the cubic hyperpolarizability of **5₂** is negative at wavelengths above 500 nm. Relative to **4-H**, **5₂** is a very active chromophore exhibiting remarkable refractive and absorptive NLO activities in the near-IR range, a performance most likely resulting from a synergistic interaction between the central Zn(TPP) core and the four peripheral carbon-rich organometallic dendrons. Comparison with the related molecules **4-H** and **7** reveals that, while the overall increase in cubic nonlinearity essentially scales with the increase in molecular size (as determined by the molecular mass) along this series of molecules, a comparably larger improvement in 2PA is found in technologically important windows: near 800 nm, in the region of maximum tissue transparency, and in the 1100-1300 nm range, close to the telecommunication window corresponding to maximum transparency of silica, highlighting the potential of extended porphyrin-based dendritic structures for enhancing third-order NLO effects in the near-IR range.

Experimental

Synthetic procedures

General. All reactions were performed under argon and were magnetically stirred. Solvents were distilled from appropriate drying agents prior to use: CH₂Cl₂ from CaH₂, CHCl₃ from P₂O₅. All other solvents were HPLC grade. Commercially available reagents were used without further purification unless otherwise stated. All reactions were monitored by thin-layer chromatography (TLC) with Merck pre-coated aluminium foil sheets (Silica gel 60 with fluorescent indicator UV₂₅₄). Compounds were visualized with ultraviolet light at 254 and 365 nm. Column chromatography was carried out using silica gel from Merck (0.063-0.200 mm). ¹H NMR, ³¹P NMR and ¹³C NMR spectra were recorded in CDCl₃ using Varian 400 MHz or Bruker 200 DPX, 300 DPX, 500 DPX, or 800 MHz spectrometers. The chemical shifts are referenced to internal tetramethylsilane. NMR spectroscopic assignments were performed with the aid of 2D NMR experiments: COSY (Correlation Spectroscopy), HMBC (Heteronuclear Multiple Bond Correlation) and HMQC (Heteronuclear Multiple Quantum Coherence). High-resolution mass spectra were recorded on a ZabSpec TOF Micromass spectrometer in FAB mode or ESI positive mode at CRMPO. IR spectra were recorded on a Bruker IFS 28 spectrometer, using KBr pellets or in dichloromethane solution. UV spectra were recorded on a UVIKON XL spectrometer. Cyclic voltammetry measurements were recorded using a e-corder 401 potentiostat system from eDaq Pty Ltd (Australia) or a VersaSAT3 from Ametek

(France). Measurements were carried out at room temperature using Pt disc working-, Pt wire auxiliary- and Ag/AgCl or SCE reference electrodes, such that the ferrocene/ferrocenium redox couple was located at 0.46 (CH_2Cl_2) or 0.56 V (THF) relative to saturated calomel electrode (i_{pc}/i_{pa} = 1, ΔE_p 0.09-0.12 V).[55] Scan rates were typically 100 mV s^{-1}. Electrochemical solutions contained 0.1 M [NBu$_4$][PF$_6$] and *ca.* 10^{-3} M complex in dried and distilled solvent. Solutions were purged and maintained under a nitrogen atmosphere.

The tetraruthenium porphyrin precursor complex **11** was obtained from the known 5,10,15,20-tetra((4-ethynyl)phenyl)porphyrinatozinc(II)[40,56] and *cis*-[RuCl$_2$(κ^2-dppe)$_2$][68] as described below, while the synthesis of the organometallic wedge **10**[18] is reported as Supporting Information.

Synthesis of the tetra-ruthenium(II) porphyrin precursor 11-v[PF$_6$]$_4$. NaPF$_6$ (95 mgs, 0.57 mmol) was added to a solution of 5,10,15,20-tetra(4-ethynylphenyl)porphyrinatozinc(II) (**6**; 100 mgs, 0.13 mmol) and *cis*-[RuCl$_2$(κ^2-dppe)$_2$] (551 mgs, 0.57 mmol) in CH_2Cl_2 (100 mL). This mixture was stirred at room temperature for 12 h and the solution was filtered. The title compound was then precipitated as a green solid by addition of Et$_2$O. This crude precipitate (478 mgs, 0.094 mmol) was used without further purification as described below. Yield: 73%. **^{31}P{^{1}H} NMR** (81 MHz, CDCl$_3$, ppm): δ = 38.8 ppm.

Synthesis of the dodecaruthenium porphyrin dendrimer 5$_2$. Triethylamine (0.05 mL) was added to a solution of **11-v**[PF$_6$]$_4$ (57 mgs, 0.011 mmol), dendron **10** (0.113 g, 0.048 mmol) and NaPF$_6$ (0.03 g, 0.18 mmol) in distilled CH_2Cl_2 (12 mL) under nitrogen. The reaction was followed by ^{31}P NMR spectroscopy, and it was complete after 48 h at room temperature. The reaction mixture was filtered, the filtrate concentrated under reduced pressure, and the product (containing traces of demetallated porphyrin) was precipitated from the filtrate following addition to hexane, yielding a green solid (90 mgs; 60%). This solid was dissolved in THF and 1 eq. Zn(OAc)$_2$•2H$_2$O was added to the solution followed by 2 drops of Et$_3$N, and the resultant solution was stirred for 4 h. Methanol was added dropwise to the solution until the pure product precipitated. The compound was collected and was dried under vacuum. Yield 48%. **^{1}H NMR** (300 MHz, CDCl$_3$, ppm): δ = 9.20 (s, 8H, $H_{\beta\text{-pyrrolic}}$), 8.05 (d, 8H, $^3J_{H,H}$ = 8.2 Hz, H_{Ar}), 7.70-6.50 (m, 572H, $H_{Ar/dppe}$), 2.70 (s, 96H, C$H_{2/dppe}$). **^{31}P{^{1}H} NMR** (121 MHz, CDCl$_3$): δ = 54.57 (broad m), 54.35 (m). **^{13}C{^{1}H} NMR** (201 MHz, CDCl$_3$, ppm): δ = 150.4, 137.2, 137.0, 134.5, 134.3, 134.2, 134.0, 133.9, 132.1, 131.9, 131.7, 131.5, 131.4, 131.3, 131.0, 130.9, 130.7, 130.0, 129.7, 129.5, 128.9, 128.7, 128.5, 128.2, 128.1, 127.5, 127.4, 127.3, 127.1, 127.0, 123.7, 123.3, 122.8, 121.1, 116.9, 116.2, 93.1, 92.6, 89.5, 87.5, 31.7, 31.6; not all signals detected/attributed due to overlap and solubility issues. **Anal.** calc. for C$_{852}$H$_{684}$N$_4$P$_{48}$Ru$_{12}$Zn: C, 74.46; H: 5.02; N: 0.41; found C: 74.35; H: 5.18; N: 0.42. **HRMS-ESI** (m/z): calcd for [C$_{208}$H$_{171}$P$_{12}$Ru$_3$]$^+$: 3345.7448, found: 3345.7405. **FT-IR** (KBr, cm^{-1}): $\bar{\upsilon}$ = 2202 (C≡C), 2051 (RuC≡C).

Materials and methods

DFT calculations. Theoretical calculations were performed at the DFT level with the Gaussian 09 package.[69] The geometric structures were fully optimized without any symmetry

constraints using the PBE0 functional with the LANL2DZ ECP basis set.[70-71] This basis set was augmented by Alrichs polarization functions for H, C, N, Si, and Zn, and Def2-TZVP polarization functions for Ru. Phenyl groups in dppe ligands were replaced by hydrogen atoms in order to reduce computational effort.

TD-DFT calculations were performed on the optimized model structures using the B3PW91 functional,[72-74] and taking into account the solvation effects of the dichloromethane solvent using PCM.[75] TD-DFT calculations using other functionals (CAM-B3LYP,[76] PBE0,[70-71] and ωBP97XD)[77] were also performed for comparison. The best fit with experiments was obtained with the B3PW91 functional.

The UV–vis spectra were simulated from the computed TD-DFT electronic transitions, each being associated with a Lorentzian function of half-height width equal to 0.20 eV. Non-normalized simulated spectra were obtained using the Molden program.[78]

Z-scan measurements. Third-order nonlinear optical properties were investigated as previously described,[42] but with some modifications. The laser system consisted of a Quantronix Integra-C3.5F pumping a Quantronix Palitra-FS optical parametric amplifier, tuneable over a wavelength range from 500 nm to 2000 nm. The output was confirmed by use of an Ocean Optics USB2000+ spectrometer (500-1000 nm) or an Ocean Optics NIR-Quest spectrometer (1000-1800 nm). The output delivered 130 fs pulse with a 1 kHz repetition rate. Coloured glass filters and a Thorlabs polarizing filter were used to remove unwanted wavelengths and the power adjusted by use of neutral density filters, attenuating it to the μJ/pulse range to obtain nonlinear phase shifts between 0.2 to 1.3 rad. The focal length of the lens used in the experiment was 75 mm, which gave 25-40 μm beam waists resulting in Rayleigh lengths sufficiently longer than that of the sample thickness that a "thin-sample" assumption was justified. Solutions of compounds in deoxygenated and distilled CH_2Cl_2 of 0.1 w/w% concentration in 1 mm glass cells were analyzed. Samples travelled down the Z-axis on a Thorlabs motorised stage between -20 and 20 mm (where 0 was the laser focus). Data were collected by three Thorlabs photodiodes, 500-900 nm with Si based detectors, 900-1300 nm with InGaAs detectors and 1300-2000 nm with amplified InGaAs detectors, monitoring the laser input, the open-aperture signal and the closed-aperture signal. Data from the detectors were fed into three channels of a Tektronix digital oscilloscope and analyzed with a custom LabVIEW program (written by Prof. M. Samoc, Wroclaw University of Technology),[79] permitting a fitting of a theoretical trace that used equations derived by Sheik-Bahae *et al.*[80] A sample of CH_2Cl_2 was run at each wavelength as an aid in referencing to a 3 mm fused silica plate; the real and imaginary components of the second hyperpolarizability (γ) of the materials were calculated assuming additivity of the nonlinear contributions of the solvent and the solute and the applicability of the Lorentz local field approximation. The values of the imaginary parts of γ were also converted into values of effective two-photon absorption cross-sections σ_2.

THG measurements. Third-harmonic generation (THG) experiments have been performed at 1.907 μm, using a commercial (SAGA from Thales Laser) Q-switched Nd^{3+}:YAG nanosecond laser operating at λ = 1064 nm, 10 Hz repetition rate and 9 ns pulse duration. The 1064 nm laser beam was focused into a 50 cm long, high pressure (50 bar) hydrogen Raman cell which shifts the fundamental beam to λ = 1.907 μm by stimulated Raman scattering (only the back-

scattered 1907 nm Raman emission was collected at a 45° incidence angle by use of a dichroic mirror, in order to eliminate most of the residual 1064 nm pump photons). A Schott RG 1000 filter was used to filter out any remaining visible light from the laser flash lamp and from anti-Stokes emission from H_2. Suitable attenuators were used to control the power of the incident beam which was focused into the THG cell with a 20 cm focal length lens (See also ESI). The measurements were carried out using a wedge-shaped cell, consisting of two fused silica windows assembled on a stainless steel support, their inner interfaces with the liquid forming a small angle α. This cell follows the classic design implemented by Levine and Bethea for electric-field induced second-harmonic generation.[81] The wedge shapes are to measure the intensity of the harmonic radiation 3ω as a function of the cell displacement, *i.e.* without changing the incidence angle, resulting in fringes with constant amplitudes, and thereby making data processing much easier than is the case for a rotating cell with parallel windows. The whole cell was translated horizontally relative to the incident beam, producing a periodic third-harmonic generation signal (Maker fringes). See ESI for more details.

Supplementary information

Detailed syntheses for alkyne precursors **9** and **10**, multinuclear NMR spectra, cyclic voltammetric data, mol file giving Cartesian coordinates for all calculated optimized geometries, molecular-orbital diagrams of **6**, **4-H'**, **5$_2$'**, **9'**, and **9**, and additional details about the nonlinear optical measurements (THG, Z-scan).

Acknowledgements

Notes and references

‡ Other closely related organometallic dendrimers containing metal-alkynyl units in their structure have been reported with Pt(II), see for example: refs.[25-26]

§ Although it is also possible to form bis-alkynyl complexes using *trans*-Ru(κ^2-dppm)$_2$ unit,[46-47] the *trans*-Ru(κ^2-dppe)$_2$ building block provides a more convenient group to afford bis(alkynyls)[48-49] and hence facilitates dendrimer constructions.

§§ We have also confirmed that this compound can be isolated from **11** (obtained by deprotonation of **11-v**[PF$_6$]$_4$), but with reduced yields.

This steric difference is subtle; no significant steric problems were suggested using SPARTAN to model the reactants, although we have successfully used this program to estimate the size of similar molecules,[52] and it was thought to provide a reasonable estimate of the size and geometry. The experimental failure to isolate the product with the shorter wedge **12** most likely results from steric problems encountered during the chloro-for-dendron metathesis reaction

taking place on the ruthenium center "en route" toward one of the putative vinylidene intermediates.

± This suggests that 2PA and RSA dominate over SA at this wavelength for **5₂** and **7**, in contrast to **4-H**, but similar to Zn(TPP).[28]

1.   S. R. Marder, *Chem. Commun.*, 2006, 131-134.
2.   S. R. Marder, in *Inorganic Materials*, eds. D. W. Bruce and D. O'Hare, Wiley & Sons, Chichester New-York Brisbane Toronto Singapore, 1992, pp. 115-164.
3.   P. N. Prasad and D. J. Williams, *Nonlinear Optical Effects in Molecules and Polymers*, John Wiley & Sons, New York, 1991.
4.   J. L. Brédas, C. Adant, P. Tackx and A. Persoons, *Chem. Rev.*, 1994, **94**, 243-278.
5.   S. R. Marder and J. W. Perry, *Adv. Mater.*, 1993, **5**, 804-814.
6.   G. S. He, L.-S. Tan, Q. Zheng and P. N. Prasad, *Chem. Rev.*, 2008, **108**, 1245-1330.
7.   D. A. Parthenopoulos and P. M. Rentzepis, *Science*, 1989, **245**, 843-845.
8.   S. Kawata, H.-B. Sun, T. Tanaka and K. Takada, *Nature*, 2001, **412**, 697-698.
9.   C. R. Mendonca, D. S. Correa, F. Marlow, T. Voss, P. Tayalia and E. Mazur, *Appl. Phys. Lett.*, 2009, **95**, 113309 (113301-113303).
10.   H. A. Collins, M. Khurana, E. H. Moriyama, A. Mariampillai, E. Dahlstedt, M. Balaz, M. K. Kuimova, M. Drobizhev, V. X. D. Yang, D. Phillips, A. Rebane, B. C. Wilson and H. L. Anderson, *Nat. Photonics*, 2008, **2**, 420-424.
11.   J. R. Starkey, A. K. Rebane, M. A. Drobizhev, F. Meng, A. Gong, A. Elliott, K. McInnerney and C. W. Spangler, *Clin. Cancer Res.*, 2008, **14**, 6564-6573.
12.   M. Khurana, E. H. Moriyama, A. Mariampillai, K. Samkoe, D. Cramb and B. C. Wilson, *J. Biomed. Opt.*, 2009, **14**, 064006/064001-064006/064014.
13.   W. Nie, *Adv. Mater.*, 1993, **5**, 520-545.
14.   H. S. Nalwa and S. Miyata, *Nonlinear Optics of Organic Molecules and Polymers*, CRC Press, New York, 1997.
15.   I. R. Whittall, A. M. McDonagh, M. G. Humphrey and M. Samoc, *Adv. Organomet. Chem.*, 1999, **43**, 349-405.
16.   H. S. Nalwa, *Adv. Mater.*, 1993, **5**, 341-358.
17.   J. P. Morrall, G. T. Dalton, M. G. Humphrey and M. Samoc, *Adv. Organomet. Chem.*, 2008, **55**, 61-136.
18.   R. L. Roberts, T. Schwich, T. C. Corkery, M. P. Cifuentes, K. A. Green, J. D. Farmer, P. J. Low, T. B. Marder, M. Samoc and M. G. Humphrey, *Adv. Mater.*, 2009, **21**, 2318-2322.
19.   M. G. Humphrey, T. Schwich, P. J. West, M. P. Cifuentes and M. Samoc, in *Comprehensive Inorganic Chemistry II - from Element to Applications*, eds. J. Reedijk and K. Poeppelmeier, Oxford: Elsevier, 2013, vol. 8, pp. 781-835.
20.   P. V. Simpson, L. A. Watson, A. Barlow, G. Wang, M. P. Cifuentes and M. G. Humphrey, *Angew. Chem. Int. Ed.* , 2016, **55**, 2387-2391
21.   K. A. Green, M. P. Cifuentes, M. Samoc and M. G. Humphrey, *Coord. Chem. Rev.*, 2011, **255**, 2530-2541.
22.   G. Grelaud, M. P. Cifuentes, F. Paul and M. G. Humphrey, *J. Organomet. Chem.*, 2014, **751**, 181-200 (150th Anniversary Special Issue).
23.   K. A. Green, M. P. Cifuentes, M. Samoc and M. G. Humphrey, *Coord. Chem. Rev.*, 2011, **255**, 2025-2038.
24.   C. E. Powell, S. K. Hurst, J. P. Morrall, M. P. Cifuentes, R. L. Roberts, M. Samoc and M. G. Humphrey, *Organometallics*, 2007, **26**, 4456-4463.
25.   S. Leininger, P. J. Stang and S. Huang, *Organometallics*, 1998, **17**, 3981-3987.
26.   S. K. Maiti, M. G. Jardim, J. Rodrigues, K. Rissanen, J. Campo and W. Wenseleers, *Organometallics*, 2013, **32**, 406–414.
27.   K. A. Green, P. V. Simpson, T. C. Corkery, M. P. Cifuentes, M. Samoc and M. G. Humphrey, *Macromol. Rapid Commun.*, 2012, **33**, 573-578.
28.   G. Boudebs, C. Cassagne, H. Wang, J.-L. Godet and C. B. de Araújo, *J. Luminescence*, 2018, **199**, 319–322.
29.   M. de Torres, S. Semin, I. Razdolski, J. Xu, J. A. A. W. Elemans, T. Rasing, A. E. Rowan and R. J. M. Nolte, *Chem. Commun.*, 2015, **51**, 2855--2858.

30. M. Pawlicki, H. A. Collins, R. G. Denning and H. L. Anderson, *Angew. Chem. Int. Ed.*, 2009, **48**, 3244-3266.

31. K. J. Thorley, J. M. Hales, H. L. Anderson and J. W. Perry, *Angew. Chem. Int. Ed.*, 2008, **47**, 7095-7098.

32. M. Calvete, G. Y. Yang and M. Hanack, *Synth. Met.*, 2004, **141**, 231–243.

33. M. Ravikanth and K. G. Ravindra, *Curr. Sci.*, 1995, **68**, 1010-1017.

34. F. Z. Henari, *J. Opt. A: Pure Appl. Opt.*, 2001, **3**, 188-190.

35. D. Dini, M. J. F. Calvete and M. Hanack, *Chem. Rev.*, 2016, **116**, 13043-13233.

36. K. J. McEwan, G. Bourhill, J. M. Robertson and H. L. Anderson, *J. Nonlinear Opt. Phys. & Mat.*, 2000, **9**, 451-468.

37. S. V. Rao, N. K. M. N. Srinivas, D. N. Rao, L. Giribabu, B. G. Maiya, R. Philip and G. R. Kumar, *Optics Commun.*, 2000, **182**, 255-264.

38. S. Drouet, A. Merhi, D. Yao, M. P. Cifuentes, M. G. Humphrey, M. Wielgus, J. Olesiak-Banska, K. Matczyszyn, M. Samoc, F. Paul and C. O. Paul-Roth, *Tetrahedron*, 2012, **68**, 10351-10359.

39. S. Drouet, A. Merhi, G. Grelaud, M. P. Cifuentes, M. G. Humphrey, K. Matczyszyn, M. Samoc, L. Toupet, C. O. Paul-Roth and F. Paul, *New J. Chem.*, 2012, **36**, 2192-2195.

40. K. Onitsuka, H. Kitajima, M. Fujimoto, A. Iuchi, F. Takei and S. Takahashi, *Chem. Commun.*, 2002, 2576-2577.

41. K. Mishiba, M. Ono, Y. Tanaka and M. Akita, *Chem. Eur. J.* , 2017, **23**, 2067-2076.

42. A. Merhi, G. Grelaud, N. Ripoche, A. Barlow, M. P. Cifuentes, M. G. Humphrey, F. Paul and C. O. Paul-Roth, *Polyhedron*, 2015, **86**, 64-70.

43. A. Merhi, G. Grelaud, K. A. Green, N. H. Minh, M. Reynolds, I. Ledoux, A. Barlow, G. Wang, M. P. Cifuentes, M. G. Humphrey, F. Paul and C. O. Paul-Roth, *Dalton Trans.*, 2015, **44**, 7748-7751.

44. S. K. Hurst, M. P. Cifuentes, A. M. McDonagh, M. G. Humphrey, M. Samoc, B. Luther-Davies, I. Asselberghs and A. Persoons, *J. Organomet. Chem.*, 2002, **642**, 259-267.

45. A. M. McDonagh, M. G. Humphrey, M. Samoc, B. Luther-Davies, S. Houbrechts, T. Wada, H. Sasabe and A. Persoons, *J. Am. Chem. Soc.*, 1999, **121**, 1405-1406.

46. A. M. McDonagh, I. R. Whittall, M. G. Humphrey, D. C. R. Hockless, B. W. Skelton and A. H. White, *J. Organomet. Chem.*, 1996, **523**, 33-40.

47. A. M. McDonagh, M. P. Cifuentes, I. R. Whittall, M. G. Humphrey, M. Samoc, B. Luther-Davies and D. C. R. Hockless, *J. Organomet. Chem.*, 1996, **526**, 99-103.

48. D. Touchard, P. Haquette, A. Daridor, A. Romero and P. H. Dixneuf, *J. Chem. Soc., Chem. Commun.*, 1994, 859-860.

49. D. Touchard, P. Haquette, A. Daridor, A. Romero and P. H. Dixneuf, *Organometallics*, 1998, **17**, 3844-3852.

50. D. Touchard, P. Haquette, S. Guesmi, L. Le Pichon, A. Daridor, L. Toupet and P. H. Dixneuf, *Organometallics*, 1997, **16**, 3640-3648.

51. K. A. Green, "Synthesis of a Second Generation Ruthenium-Alkynyl Dendrimer", Hons Thesis, Dept of Chemistry, ANU, 2005.

52. A. M. McDonagh, C. E. Powell, J. P. Morrall, M. P. Cifuentes and M. G. Humphrey, *Organometallics*, 2003, **22**, 1402-1413.

53. S. K. Hurst, M. P. Cifuentes and M. G. Humphrey, *Organometallics*, 2002, **21**, 2353-2355 and refs therein.

54. M. P. Cifuentes, M. G. Humphrey, J. P. Morrall, M. Samoc, F. Paul, T. Roisnel and C. Lapinte, *Organometallics*, 2005, **24**, 4280-4288.

55. N. G. Connelly and W. E. Geiger, *Chem. Rev.*, 1996, **96**, 877-910.

56. S. Drouet, A. Merhi, G. Argouarch, F. Paul, O. Mongin, M. Blanchard-Desce and C. O. Paul-Roth, *Tetrahedron*, 2012, **68**, 98-105.

57. A. Merhi, X. Zhang, D. Yao, S. Drouet, O. Mongin, F. Paul, J. A. G. Williams, M. A. Fox and C. O. Paul-Roth, *Dalton Trans.*, 2015, **44**, 9470-9485.

58. M. P. Cifuentes, C. E. Powell, M. G. Humphrey, G. A. Heath, M. Samoc and B. Luther-Davies, *J. Phys. Chem. A*, 2001, **105**, 9625-9627.

59. N. Gauthier, G. Argouarch, F. Paul, L. Toupet, A. Ladjarafi, K. Costuas, J.-F. Halet, M. Samoc, M. P. Cifuentes, T. C. Corkery and M. G. Humphrey, *Chem. Eur. J.*, 2011, **17**, 5561-5577.

60. C. E. Powell, M. P. Cifuentes, J. P. Morrall, R. Stranger, M. G. Humphrey, M. Samoc, B. Luther-Davies and G. A. Heath, *J. Am. Chem. Soc.*, 2003, **125**, 602-610.
61. A. Ladjarafi, K. Costuas, H. Meghezzi and J.-F. Halet, *J. Mol. Model.* , 2015, **21**, 71-71–71-10.
62. S. J. Silvers and A. Tulinsky, *J. Am. Chem. Soc.*, 1967, **89**, 3331-3337.
63. S. Marques-Gonzalez, M. Parthey, D. S. Yufit, J. A. K. Howard, M. Kaupp and P. J. Low, *Organometallics*, 2014, **33**, 4947-4963 and refs therein.
64. N. Gauthier, N. Tchouar, F. Justaud, G. Argouarch, M. P. Cifuentes, L. Toupet, D. Touchard, J.-F. Halet, S. Rigaut, M. G. Humphrey, K. Costuas and F. Paul, *Organometallics*, 2009, **28**, 2253-2266 and refs therein.
65. A. B. J. Parusel and S. Grimme, *J. Porphyrins Phthalocyanines*, 2001, **5**, 225-232.
66. J. M. Hales, J. Matichak, S. Barlow, S. Ohira, K. Yesudas, J.-L. Brédas, J. W. Perry and S. R. Marder, *Science*, 2010, **327**, 1485-1488.
67. C. W. Spangler, *J. Mater. Chem.*, 1999, **9**, 2013-2020.
68. K. A. Green, M. P. Cifuentes, T. C. Corkery, M. Samoc and M. G. Humphrey, *Angew. Chem., Int. Ed. Engl.*, 2009, **48**, 7867-7870.
69. M. J. Frisch, G. W. Trucks, H. B. Schlegel, G. E. Scuseria, M. A. Robb, J. R. Cheeseman, G. Scalmani, V. Barone, G. A. Petersson, H. Nakatsuji, X. Li, M. Caricato, A. Marenich, J. Bloino, B. G. Janesko, R. Gomperts, B. Mennucci, H. P. Hratchian, J. V. Ortiz, A. F. Izmaylov, J. L. Sonnenberg, D. Williams-Young, F. Ding, F. Lipparini, F. Egidi, J. Goings, B. Peng, A. Petrone, T. Henderson, D. Ranasinghe, V. G. Zakrzewski, J. Gao, N. Rega, G. Zheng, W. Liang, M. Hada, M. Ehara, K. Toyota, R. Fukuda, J. Hasegawa, M. Ishida, T. Nakajima, Y. Honda, O. Kitao, H. Nakai, T. Vreven, K. Throssell, J. A. Montgomery, Jr., J. E. Peralta, F. Ogliaro, M. Bearpark, J. J. Heyd, E. Brothers, K. N. Kudin, V. N. Staroverov, T. Keith, R. Kobayashi, J. Normand, K. Raghavachari, A. Rendell, J. C. Burant, S. S. Iyengar, J. Tomasi, M. Cossi, J. M. Millam, M. Klene, C. Adamo, R. Cammi, J. W. Ochterski, R. L. Martin, K. Morokuma, O. Farkas, J. B. Foresman and D. J. Fox, *Gaussian 16 Rev. B.01*, Gaussian, Inc. Wallingfort CT, 2016.
70. C. Adamo and V. Barone, *Chem. Phys. Lett.*, 1997, **274**, 242-250.
71. C. Adamo and V. Barone, *J. Chem. Phys.*, 1999, **110**, 6158-6178.
72. J. P. Perdew, *Phys. Rev. B*, 1986, **33**, 8822-8824.
73. A. D. Becke, *J. Chem. Phys.*, 1993, **98**, 5648-5652.
74. J. P. Perdew, K. Burke and Y. Wang, *Phys. Rev. B*, 1996, **54**, 16533-16539.
75. J. Tomasi, B. Mennucci and R. Cammi, *Chem. Rev.*, 2005, **105**, 2999-3093.
76. T. Yanai, D. P. Tew and N. C. Handy, *Chem. Phys. Lett.*, 2004, **393**, 51-57.
77. J.-D. Chai and M. Head-Gordon, *Phys. Chem. Chem. Phys.* , 2008, **10**, 6615-6620.
78. G. Schaftenaar and J. H. Noordik, *J. Comput.-Aided Mol. Design* 2000, **14**, 123-134.
79. M. Samoc, A. Samoc, B. Luther-Davies, M. G. Humphrey and M. S. Wong, *Opt. Mater.*, 2003, **21**, 485-488.
80. M. Sheikh-Bahae, A. A. Said, T. Wei, D. J. Hagan and E. W. V. Stryland, *IEEE J. Quant. Electr.*, 1990, **26**, 760-769.
81. B. F. Levine and C. G. Bethea, *J. Chem. Phys.*, 1975, **63**, 2666-2682.